JOURNAL OF AIRCRAFT
Vol. 39, No. 4, July–August 2002

Rotor Wake Study Near the Horizontal Tail of a T-Tail Configuration

Susan Althoff Gorton*
NASA Langley Research Center, Hampton, Virginia 23681-2199
John D. Berry†
U.S. Army Aviation and Missile Command, Redstone Arsenal, Alabama 35898-5000
and
W. Todd Hodges‡ and Deane G. Reis‡
U.S. Army Aviation and Missile Command, Hampton, Virginia 23681-2199

Development of advanced rotorcraft configurations has highlighted a need for high-quality experimental data to support the development of robust and accurate analytical design tools. To provide high-quality experimental data, a test program was conducted in the NASA Langley Research Center 14- by 22-Foot Subsonic Tunnel to measure the flow near the empennage of a 15% scale powered helicopter model with an operating tail fan and a T-tail configuration. Three-component velocity profiles were measured forward of the horizontal tail for four advance ratios using laser velocimetry to evaluate the effect of the rotor wake impingement on the horizontal tail angle of attack. These velocity data indicate the horizontal tail can experience unsteady angle-of-attack variations of over 30 deg due to the rotor wake influence. The horizontal tail is most affected by the rotor wake at and above advance ratios of 0.10.

Nomenclature

C_T	=	rotor thrust coefficient, $T/\rho\pi R^2(\Omega R)^2$
R	=	rotor radius, ft
T	=	rotor thrust, lb
U_∞	=	freestream velocity, ft/s
u	=	streamwise component of velocity, ft/s
v	=	lateral component of velocity, ft/s
v_f	=	induced velocity in forward flight, ft/s
v_h	=	induced velocity in hover, ft/s
w	=	vertical component of velocity, ft/s
X	=	wake skew angle, $\tan^{-1}\{U_\infty\cos(\alpha)/[v_f - U_\infty\sin(\alpha)]\}$, deg
x, y, z	=	Cartesian coordinates (Fig. 3), in.
α	=	rotor shaft angle, positive nose up, deg
μ	=	main rotor advance ratio, $U_\infty/\Omega R$
ρ	=	Density of air, slug/ft^3
Ω	=	main rotor rotational speed, rad/s

Introduction

As rotor and fuselage designs become more integrated, compact, and complex, rotor–wake–fuselage aerodynamic interactions are an increasingly important part of the overall performance characteristics of rotorcraft. In Ref. 1, the importance of interactional effects for modern helicopters is attributed to increased disk loading, more compact designs, low-level flight requirements, and the increased requirement for directional trim after the loss of the tail rotor that results in larger vertical tail surfaces. These effects are especially important in the design and placement of the antitorque system, such as a tail rotor, and the horizontal and vertical stabilizers, as documented in Refs. 2 and 3.

Much work has already been done experimentally and analytically to define the interaction effects between the rotor and the fuselage.[4–15] However, prediction of the unsteady interactional effects of the main rotor wake on the fuselage and empennage are not yet developed to the point where they can be used as a preliminary design tool. In fact, many advanced analysis methods in use are time-averaged solutions,[16,17] due to the extemely large computational requirements required to track the individual rotor tip vortices.[18] Projections of advances in computational capability[19,20] indicate that hybrid methods of analysis may be the best tradeoff between high-fidelity simulation and computational resources; however, the use of these methods usually results in the acceptance of a time-averaged solution away from the nearfield of the rotor. In Ref. 21, a method that models the unsteady effects of the rotor on the fuselage is demonstrated, but the method has not been fully validated for empennage interactions and may have some of the same vorticity dissipation issues as other methods in the far field.

A limited amount of experimental data are available for analyzing the main rotor–antitorque interactions,[22–28] and unsteady velocity flowfield data are a subset within these data sets. Advanced configurations such as the reconnaissance attack helicopter 66 (RAH-66) are designed and manufactured with new and sophisticated antitorque devices, and there is a need for high-quality experimental data to support the development of more flexible analytical models capable of treating these types of configurations.[29,30] In Ref. 31 the difficulty in predicting unsteady empennage loads at speeds below 40 kn is specifically cited. In Ref. 32, experimental pressure data at model scale for a generic T-tail empennage are provided, and in Ref. 33 the tremendous amount of testing involved in the light helicopter design process is discussed. However, there does not appear to be specific information in the literature on the steady or unsteady velocities in the flowfield for the particular combination of a lifting rotor near an operating tail fan with a T-tail empennage.

To investigate the rotor wake–fuselage–empennage interactions near the empennage of a powered small-scale helicopter with an operating tail fan and a T tail, the U.S. Army Joint Research Program Office, Aeroflightdynamics Directorate, in cooperation with NASA

Received 6 August 2001; revision received 23 April 2002; accepted for publication 23 April 2002.

*Aerospace Engineer, Flow Physics and Control Branch, Mail Stop 170. Member AIAA.
†Chief, Rotor Dynamics and Aerodynamics Branch Aeromechanics Division, Aviation Engineering Directorate, Building 4488, Room B379.
‡Aerospace Engineer, Joint Research Program Office, Aeroflightdynamics Directorate, Mail Stop 286.

Langley Research Center, conducted a wind-tunnel test program in the 14- by 22-Foot Subsonic Tunnel during 1995. Velocity data were acquired forward of the horizontal tail for four flight conditions to document the unsteady downwash and sidewash velocities near the horizontal tail. These data were to be used for calibrating current analyses, evaluating methodolgies under development, and supporting the analysis of configurations such as the RAH-66.

Model and Instrumentation

The test program was conducted in the NASA Langley Research Center 14- by 22-Foot Subsonic Tunnel using the Army's 2-Meter Rotor Test System (2MRTS) with a four-bladed, 15% scale rotor, a fuselage model representative of the RAH-66, and a three-component laser velocimetry (LV) system.

The 14- by 22-Foot Subsonic Tunnel is a closed-circuit, atmospheric wind tunnel designed for the low-speed testing of powered and high-lift configurations.[34] In the open test section configuration, the walls and ceiling are lifted out of the flow, leaving a solid floor under the model. In this configuration, the tunnel can achieve a maximum dynamic pressure of about 92 lb/ft^2. This investigation was conducted with the tunnel in the open test section configuration to allow complete optical access to the rotor flowfield. For this test program, the test section floor was lowered 2 ft to install the third component LV optics. A false floor with a window, flush with the rest of the tunnel, was placed over the LV optics.

Figure 1 shows the 2MRTS ready for testing in the tunnel. The LV system is also visible in the photograph. The rotor system, which was installed on the 2MRTS, had a four-bladed, articulated hub with blades that closely matched the planform, twist, and airfoils of the RAH-66 blades. No attempt was made to scale these blades dynamically. Because the only hub available for testing was a four-bladed hub, there were some deviations of scale from an actual model of the five-bladed RAH-66. The radius of the blades when installed on the four-bladed hub was reduced by 1 in. from a true 15% scale RAH-66. In addition, the use of only four blades reduced the rotor solidity and resulted in higher blade loads for any given thrust coefficient. The blades and hub are described in more detail in Table 1, and the blade planform is shown in Fig. 2. The 2MRTS is described in further detail in Ref. 35.

The fuselage was a 15% scale model of the RAH-66 and was instrumented with over 200 surface pressure ports and 4 dynamic pressure gauges. Forces and moments on the rotor and fuselage were measured separately by two six-component, strain-gauge balances. The fuselage is shown in detail in Fig. 3. Fuselage surface pressure data were acquired during this test program, and samples of the pressure data are used in Ref. 36 for computational fluid dynamics code calibration.

The antitorque device of the configuration was modeled by an air-powered, tip-driven, 8-in.-diam, 22-bladed fan mounted in the tail fan duct. The fan configuration is shown in Fig. 4. As shown in the photograph, the fan duct section was painted black to minimize the optical reflections from the surface. Although the fan configuration did not match the physical eight-bladed tail fan assembly of the full-scale configuration, the model fan was used to simulate the general flow physics and trim conditions for the model by using the fan revolutions per minute to control the fan thrust. For this study, a general simulation of the thrusting fan environment was thought to be sufficient to yield information regarding the flowfield around the fuselage and empennage. Obviously, a detailed assessment of the full-scale fan design could not be made using this type of simulation.

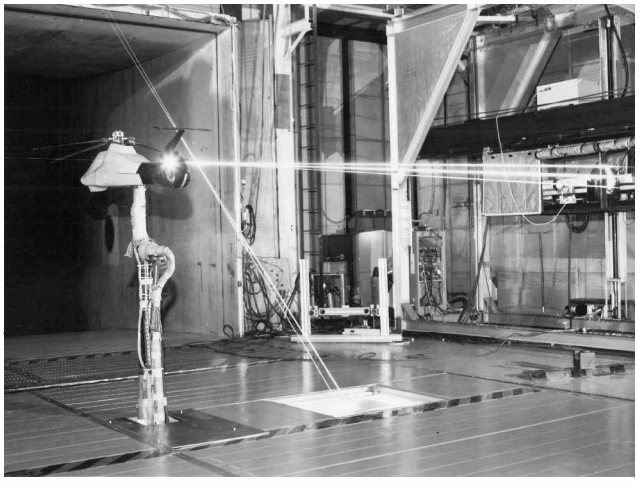

Fig. 1 Model and LV system installed in tunnel.

Laser Velocimeter System and Data Acquisition

The LV system was a three-component system operated in the backscatter mode to minimize alignment difficulties between the transmit and receive optics packages. Most components of the system are described in Refs. 37 and 38; this paper presents the first data obtained with the upgraded three-component system floor. The streamwise and vertical components of velocity are measured by optics located on the side of the tunnel, out of the flow; the lateral crossflow component of velocity is measured by optics that are located beneath the tunnel floor. The traversing mechanisms of the three components are computer controlled to ensure the sample volumes of the three sets of beams are positioned at a single location.

Table 1 Description of rotor blades

Property	Value
Airfoil sections	
23.7% radius	VR-12[a]
84.6% radius	VR-12
91.8% radius	SSC-A09[b]
100% radius	SSC-A09
Chord, in.	
23.7% radius	2.25
74.3% radius	2.25
91.8% radius	2.25
100% radius	1.35
Cutout, in.	8.2
Flapping hinge offset, in.	2.0
Lag hinge offset, in.	2.0
Number of blades	4
Pitch axis, percent of chord	25
Radius, in.	34.55
Solidity, thrust-weighted	0.07866
Tip sweep angle (of $\frac{1}{4}$ chord), deg	30
Tip sweep begins, in.	31.7
Twist, deg	
0% radius	0
23.7% radius	0
74.3% radius	−6.6
84.6% radius	−7.6
91.8% radius	−9.5
100% radius	−9.5

[a]The Boeing Company airfoil, 12% thick.
[b]Sikorsky airfoil, 9% thick.

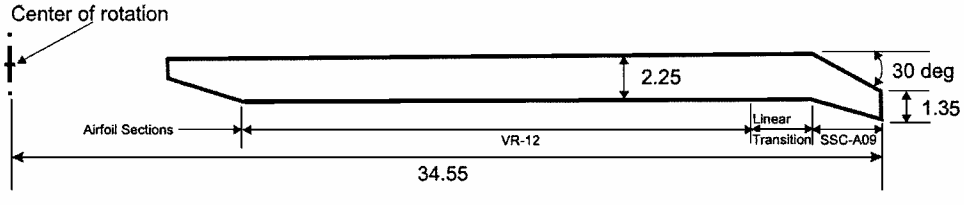

Fig. 2 Blade planform; all dimensions in inches.

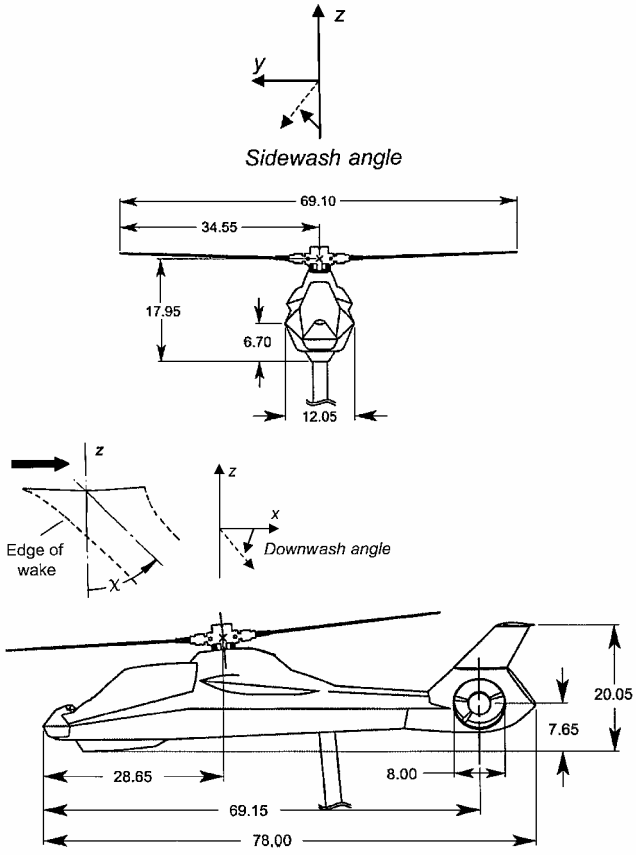

Fig. 3 Description of fuselage and axis system; all dimensions in inches.

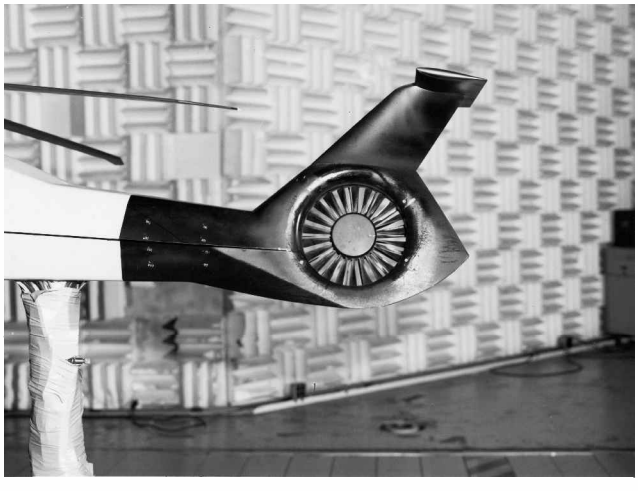

Fig. 4 Tail fan configuration.

As can be seen in Fig. 1, the third-component beams originating beneath the floor were angled at 33 deg relative to the vertical. This angle was necessary to access optically the measurement area due to the cant of the tail fan duct. Corrections for this rotation in the lateral velocity component were applied to the data during postprocessing. The sample volume diameter for the three-component system was approximately 0.2 mm for each of the components. The length of the sample volume, transverse to the flow direction for each component, was less than 5 mm as measured using a microscope objective and optical filtering glasses, and it was verified through the receive optics using a small, portable seed generator. Although this would be considered a large sample volume for a typical LV system, it was considered acceptable for an LV system with a 7-m focal length.

Except for its long focal length and zoom lens assembly, the system was a standard fringe-based LV system. Polystyrene particles (1.7 μm) suspended in an alcohol and water mixture were used to seed the flow. The velocity data were acquired using frequency-domain processors (FDPs) to maximize the signal-to-noise ratio of the data. To improve the accuracy of the measurements and minimize spatial velocity gradient bias, the FDPs were operated with a high validation ratio required; this ensured the measurements were being made at the highest signal level in the center of the sample volume. The LV data acquisition system was designed to allow acquisition of rotor azimuth position in addition to the velocity measurements so that an azimuthal history of the velocity could be reconstructed in postprocessing.

The LV data acquisition process consisted of positioning the sample volume at the measurement location and acquiring data for a period of 9 min or until 4096 velocity measurements were made in each of the longitudinal, vertical, and lateral components of velocity. The LV measurements were not made in coincidence, which would have required that each component of velocity be measured at the same time from the same particle. Instead, the flow was assumed to be periodic with rotor blade passage, and each component was allowed to be measured individually; this dramatically reduced the time required to obtain the LV data. During this process, as was mentioned earlier, conditional sampling techniques were employed to associate each measured velocity with the azimuth of the rotor blades at the time when the measurement was made. At the conclusion of the process, the measurement location was changed, and the acquisition process was repeated.

For each measurement location, the raw data were reviewed, and the histograms of the velocities in each of the three components were processed to improve the signal-to-noise ratio. Because many of these histograms were double peaked due to close vortex passage, a simple three-sigma processing algorithm would not have been valid. Therefore, the processing was accomplished by reviewing the velocity histogram at each location for each component and discriminating outlying data using a combination of three-sigma criterion and engineering judgement based on the histogram statistics. The data were binned into 128 bins (2.8 deg azimuth each), and the mean velocity for the location was calculated from the mean of all of the azimuth bins. Because the data were associated with a rotor position, it was possible to sort the data by azimuthal position, thereby reconstructing a time history of velocity at each measurement location that represented one average rotor revolution. The reconstruction of the rotor revolution confirmed the original assumption that the flow was periodic.

Measurement Uncertainty

Wind-tunnel wall interference corrections were calculated using the methods of Ref. 39 and were found to be negligible for this configuration. The uncertainties associated with the wind-tunnel standard measurements were calculated using the method of Ref. 40, and they are documented in Table 2. The uncertainty in the performance data that were measured with the balances is also given in Table 2, as well as the uncertainty in the rotor control angles. Both bias and random error sources that were evaluated for the LV measurements were crossbeam angle measurement error, velocity bias, Bragg bias, velocity gradient, FDP error, and particle lag. The largest contributors to the uncertainty in the LV velocity measurements are the measurement of the crossbeam angle and the particle lag. When the error estimation techniques described in Refs. 37, 41, and 42 are used, the LV system error for the velocity measurements in this paper is estimated at 1.3% measured velocity.

Measurement Locations

The laser velocimeter measurement locations are described briefly subsequently and are shown in Fig. 5. The operating conditions for each configuration are documented in Table 3. LV data were obtained for 11 points evenly spaced over 5 in. in a vertical line one chord forward and one chord (midsemispan) to the right of center of the horizontal tail with both the main rotor and tail fan operating for main rotor advance ratios of 0.055, 0.076, 0.102, and 0.150. The rotor thrust coefficient was 0.007, and the rotor shaft angle was held at a constant −0.65 deg.

Table 2 Measurement uncertainty

Measurement	Uncertainty
Advance ratio	±0.0011
Collective, deg	±0.5
Density, slug/ft^3	±0.000003
Fuselage angle of attack, deg	±0.001
Freestream velocity, ft/s	±0.274
Fuselage yaw moment, in. · lb	±1.5
Lateral cyclic, deg	±0.5
Longitudinal cyclic, deg	±0.5
Rotor drag, lb	±0.4
Rotor lift, lb	±1.0
Rotor, rpm	±2
Rotor shaft angle, deg	±0.001
Rotor thrust coefficient	±0.00037
Rotor yawing moment, in. · lb	±12.0
Tail fan, rpm	±40
Dynamic pressure, lb/ft^2	±0.083
Ambient temperature, °F	±0.54
Dew point temperature, °F	±0.54
Total pressure, lb/ft^2	±0.92
LV velocity measurements, ft/s	±1.3%

Table 3 Test conditions

Variable	Test condition			
Advance ratio	0.055	0.076	0.102	0.15
Collective, deg	11.0	10.1	8.9	7.5
Density, slug/ft^3	0.00236	0.00237	0.00236	0.00235
Fuselage angle of attack, deg	4.1	4.0	4.1	4.1
Freestream velocity, ft/s	40.0	54.7	73.8	108.9
Freestream velocity, kn	23.7	32.4	43.7	64.5
Fuselage yaw moment, in. · lb	−473.4	−631.3	−815.5	−781.4
Lateral cyclic, deg	1.2	1.3	1.9	2.5
Longitudinal cyclic, deg	−2.8	−3.0	−3.2	−2.7
Rotor drag, lb	0.6	2.8	2.6	3.3
Rotor lift, lb	230.5	228.9	229.4	228.8
Rotor, rpm	2400	2399	2402	2401
Rotor shaft angle, deg	−0.66	−0.61	−0.61	−0.61
Rotor thrust coefficient	0.00714	0.00706	0.00707	0.00709
Rotor yawing moment, in. · lb	540.3	497.2	421.8	310.0
Tail fan, rpm	4860	5197	6262	5435

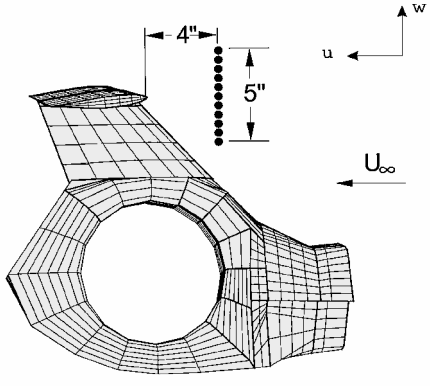

Side view of horizontal tail measurement locations

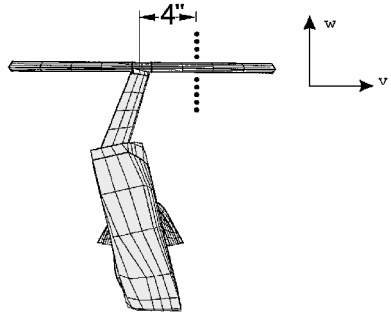

Rear view of horizontal tail measurement locations

Fig. 5 Velocity measurement locations; all dimensions in inches.

Discussion of Results

The LV velocity data acquired at each measurement location one chord forward of the horizontal tail were used to calculate the downwash and sidewash angles for each test condition. For each measurement location, an average downwash and sidewash angle were computed based on the averaged values of the velocity over the rotor revolution. The average downwash angle is shown in Fig. 6 for several advance ratios, and the average sidewash

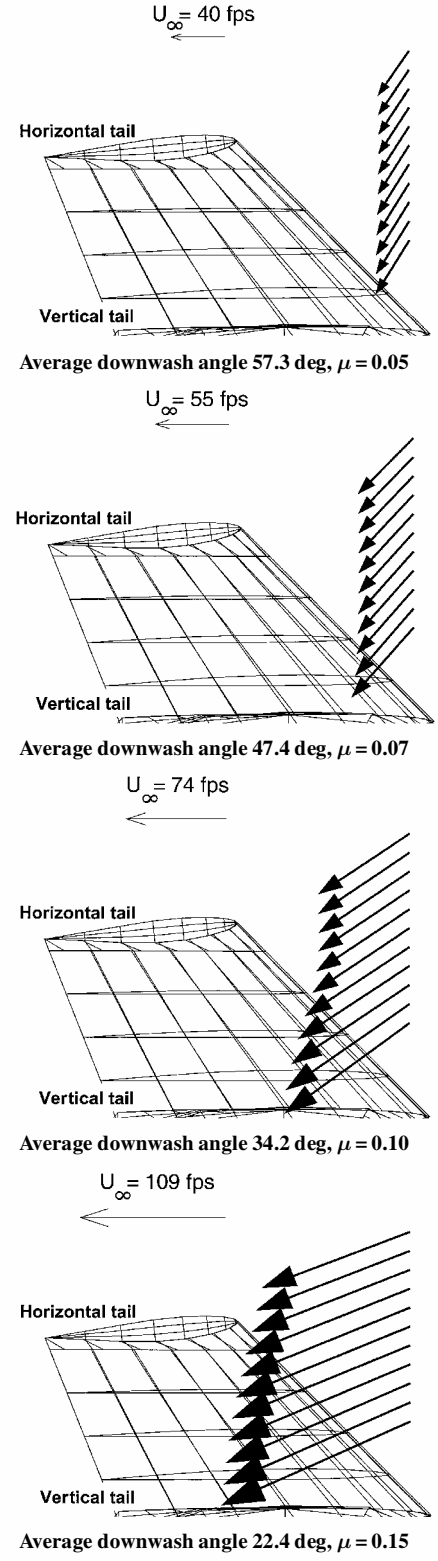

Fig. 6 Average downwash angle forward of the horizontal tail; view from right side of model.

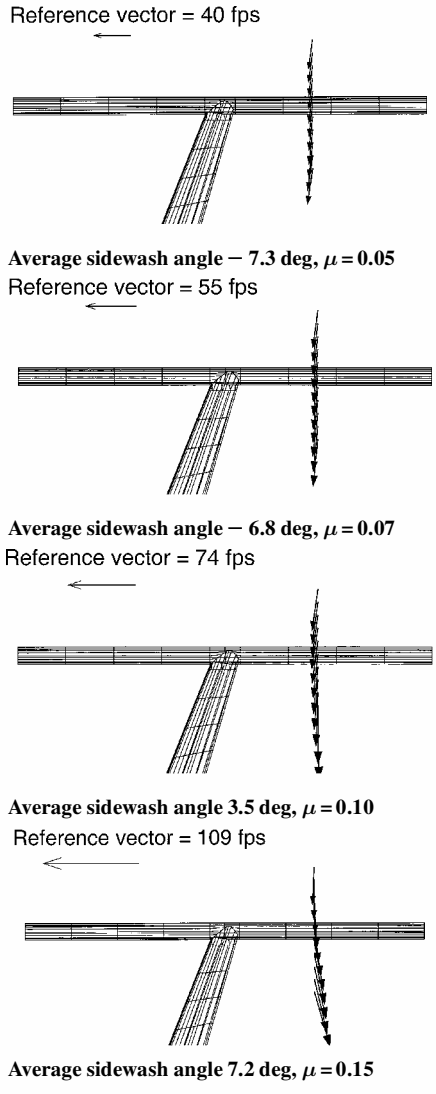

Fig. 7 Average sidewash angle forward of the horizontal tail; view from rear of model.

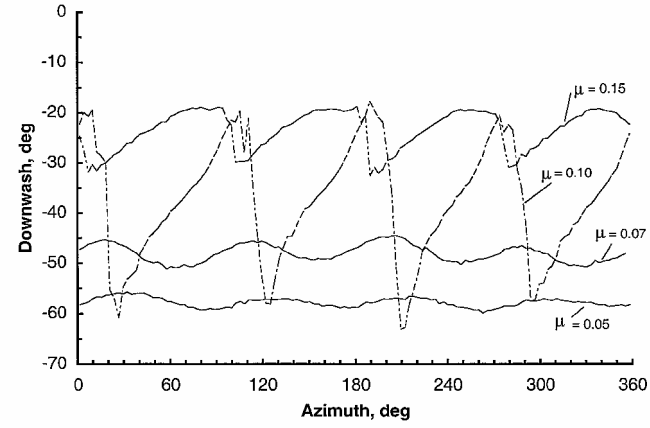

Downwash angle, positive downwash is positive z direction

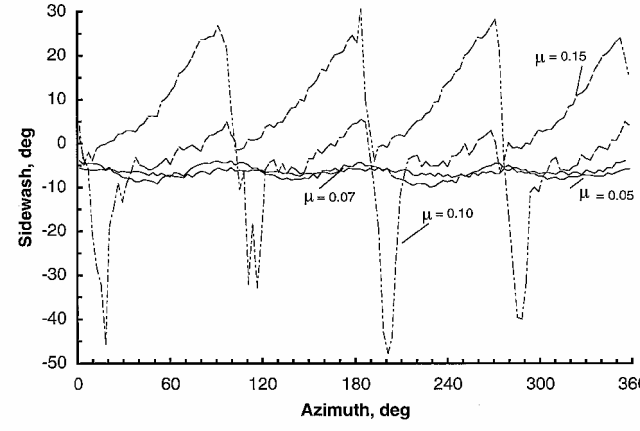

Sidewash angle, positive sidewash is positive y direction

Fig. 8 Unsteady angles for a location 0.5 in. below the horizontal tail.

angle is shown in Fig. 7. In each of these cases, both the main rotor and the tail fan are operating at the conditions indicated in Table 3. Figures 6 and 7 also indicate an overall averaged downwash or sidewash for the specified test conditions. This average for the test condition was calculated by averaging the angles for the individual measurements at that condition. As expected, the downwash angle decreases with increasing advance ratio. Similarly, the average sidewash angle is shown in Fig. 7. The sidewash angle increases with increasing advance ratio, that is, the average lateral flow tends more to the starboard side of the model with increasing forward speed.

Extremely large variations in the unsteady downwash and sidewash angles were also measured using the LV system. Typical plots of the unsteady flow angles calculated from the unsteady velocity data are shown in Fig. 8 for a height $\frac{1}{2}$ in. below the horizontal tail for each of the advance ratios tested. The results indicate over 30 deg of unsteady fluctuation are encountered near the horizontal tail at the blade passage frequency with the most unsteadiness occurring at an advance ratio of 0.10. Carpet plots of the unsteady angles for all of the advance ratios that were tested are presented in Fig. 9. These plots show the variation in unsteady angle with height above the tail section at each advance ratio. In Fig. 9, the dynamic flow environment near the horizontal tail is apparent by the wide range of magnitude seen in the downwash and sidewash velocities. The magnitude of these angle excursions was unexpected and was due to the large, concentrated vorticity convected past the tail in the tightly formed tip vortices. The ability to predict this type of flow environment using unsteady, time-accurate, vortex-dominated calculations is still an area of research.[18–21] However, it is seen from the unsteady data that a time-averaged solution for the flow environment will miss a substantial portion of the flowfield.

From the unsteady data, an experimental determination of the position of the rotor wake relative to the horizontal tail can be made by analyzing the 4 per revolution content of the velocity. The vertical component of velocity was used to calculate the 4 per revolution rms content of the rotor wake, and the results are shown in Fig. 10. The strong 4 per revolution content indicates that the rotor wake is the dominant flow feature. In Fig. 10, the shaded bars also show the position of the rotor wake relative to the horizontal tail for the advance ratios tested. In Fig. 10, the tail is immersed in the wake above advance ratios of 0.10 as shown by the high 4 per revolution content at all measurement locations for these advance ratios. These results generally agree with those in Ref. 32, considering the different geometry and flight conditions of the two test configurations. This general agreement indicates that the operating tail fan had an insignificant effect on the interaction of the main rotor wake and the T tail, although the influence of the rotor wake on the tail fan and shroud is documented in Ref. 43.

Often preliminary design analysis is based on fairly simple rotor analysis theory to provide quick design evaluations. Wake skew angle is one of the basic rotorcraft design parameters that determine the operational envelope in which the main rotor wake will impinge on the fuselage and the empennage. It is a generally accepted practice to calculate wake skew angle initially based on the equations in Ref. 44 to evaluate the initial placement of the control surfaces. It is also standard to use the hover-induced velocity v_h, in the equation for wake skew angle for both hover and forward flight. Because v_h is defined as

$$v_h = \sqrt{T/2\rho\pi R^2} \tag{1}$$

this is a fairly straightforward calculation. However, when the wake skew angle for a forward-flight configuration is determined, the induced velocity in forward flight v_f can be shown to be a function of thrust, tip speed and forward speed. The dependence on forward speed is not accounted for in Eq. (1). When the Eqs. of Ref. 44 are solved, and the rotor shaft angle is assumed to be small, v_f is given by

$$v_f = 1/\sqrt{2}\sqrt{\left(\sqrt{\left[C_T^2(\Omega R)^4 + U_\infty^4\right]} - U_\infty^2\right)} \tag{2}$$

The skew angle for forward flight is then calculated by

$$X = \tan^{-1}\left[\frac{U_\infty \cos(\alpha)}{v_f - U_\infty \sin(\alpha)}\right] \tag{3}$$

This formulation in Eq. (3) using the forward-flight-induced velocity results in a significantly different skew angle calculation than if the hover value of induced velocity is used as shown in Table 4. The results of the skew angle calculation using the forward-flight-induced velocity are plotted in Fig. 11 along with the geometry of the configuration. Figure 11 shows a very simplistic representation of the complex rotor wake system. In Ref. 45, it is explained in much more detail, using flow visualization and quantitative measurements of rotor wake parameters, how the wake system convects downstream into the tail region. In Ref. 45, the existence is shown of an edge of the wake defined by the tip vortices as they wrap around the disk vortices. This edge can be generally approximated by the calculation of skew angle initiating from the trailing edge of the rotor disk. In Fig. 11, the calculated wake skew angle, which theoretically defines the upper edge of the rotor wake, is plotted for each of the four forward speeds. Figure 11 shows the wake generated from the aft portion of the rotor disk, the trajectory of the wake through the LV measurement locations, and the possible impingement locations

Table 4 Skew angle comparison

Advance ratio	Skew angle, deg: From hover-induced velocity	Skew angle, deg: From forward-flight-induced velocity
0.05	26	49
0.07	34	62
0.10	44	72
0.15	55	81

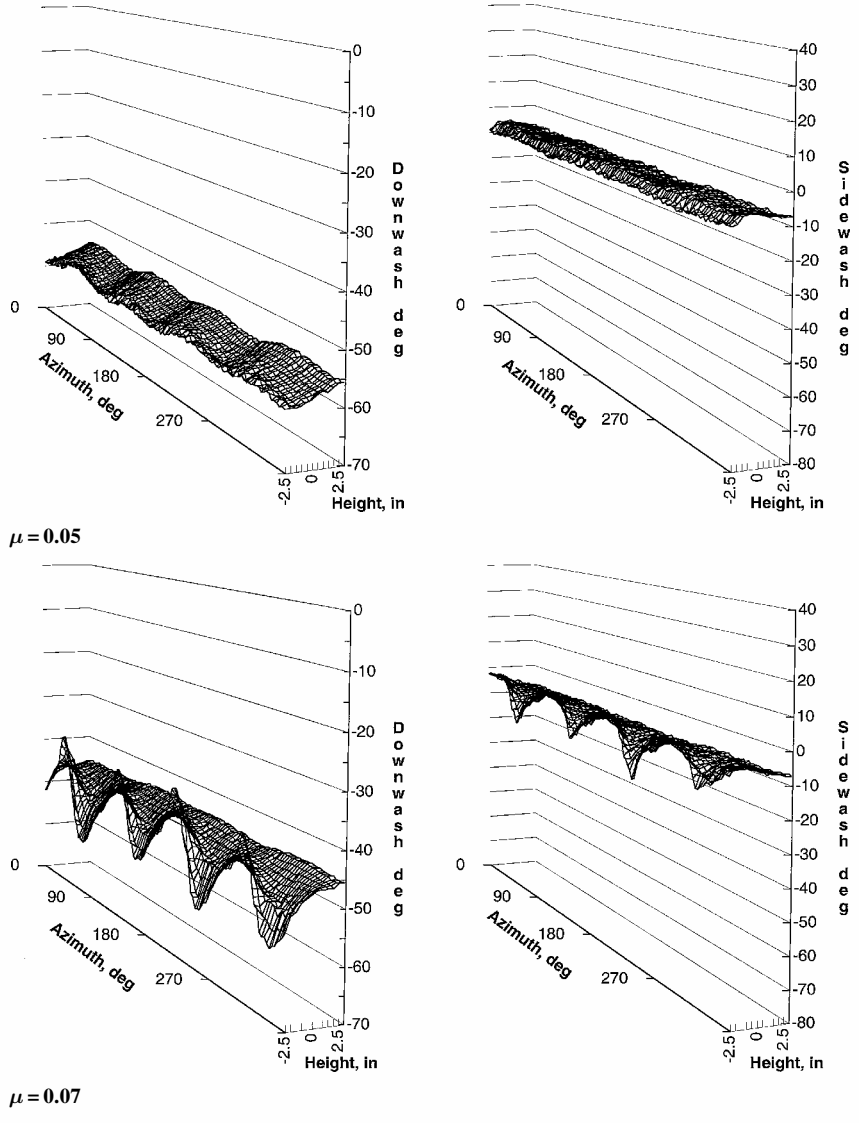

Fig. 9 Unsteady downwash and sidewash angles.

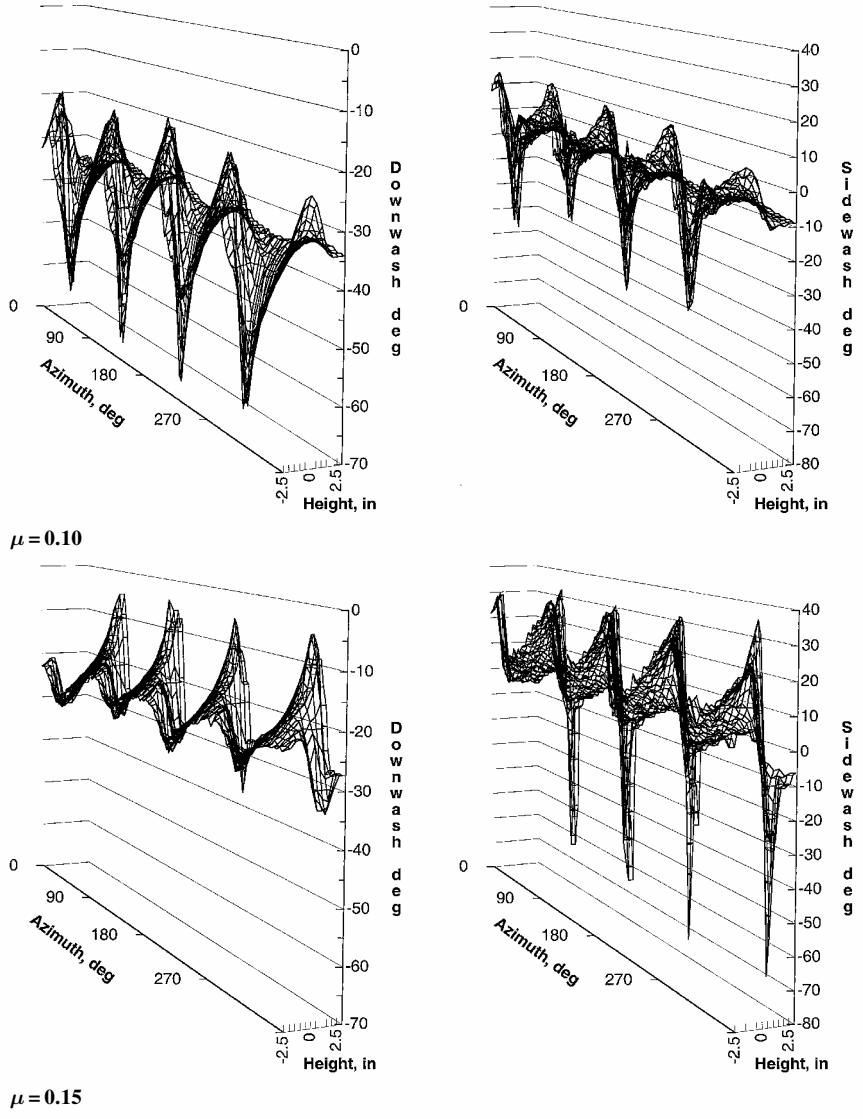

Fig. 9 Unsteady downwash and sidewash angles (continued).

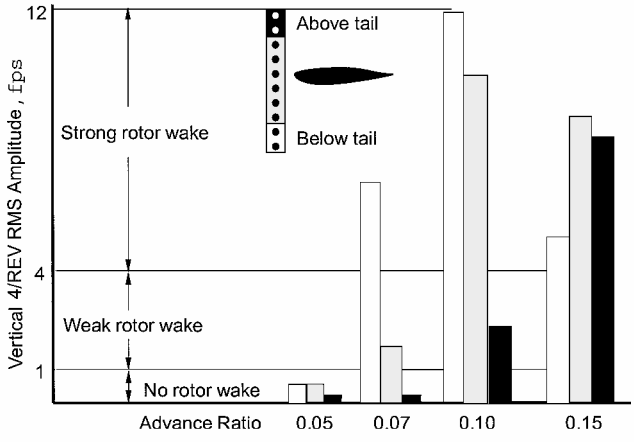

Fig. 10 Unsteady vertical wake impingement at horizontal tail.

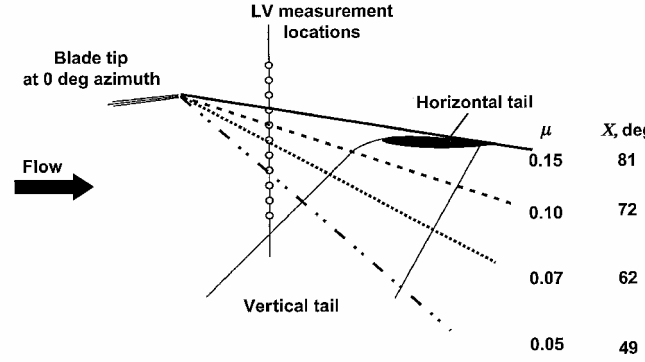

Fig. 11 Wake skew angle calculation for $C_T = 0.007$ projected on model geometry; view from left side of model: ——, $\mu = 0.15$, $X = 81$ deg; – – –, $\mu = 0.10$, $X = 72$ deg; · · ·, $\mu = 0.07$, $X = 62$ deg; and –···–, $\mu = 0.05$, $X = 49$.

on the horizontal and vertical tails. The wake is shown to approach the position of the horizontal T tail at advance ratios of 0.10 and above. This correlates well with the experimental determination of rotor wake position shown in Fig. 10. Note that the skew angle from Table 4 calculated using hover-induced velocity would have been greatly in error predicting the location of the rotor wake.

Figure 12 shows an interesting feature of the unsteady vertical flow near the horizontal tail. At the lower advance ratios of the test program, represented by the sample plot in Fig. 12a, the flow is dominated by the 4 per revolution blade passage frequency and its multiples. At an advance ratio of 0.15, a significant 2 per revolution content becomes present in the flow as shown in Fig. 12b. In Ref. 32, a strong 8 per revolution in the flow near the horizontal tail is also reported; the data in the present investigation show periodic content at several multiples of the 4 per revolution frequency, as well as frequencies between the multiples of the 4 per revolution. During

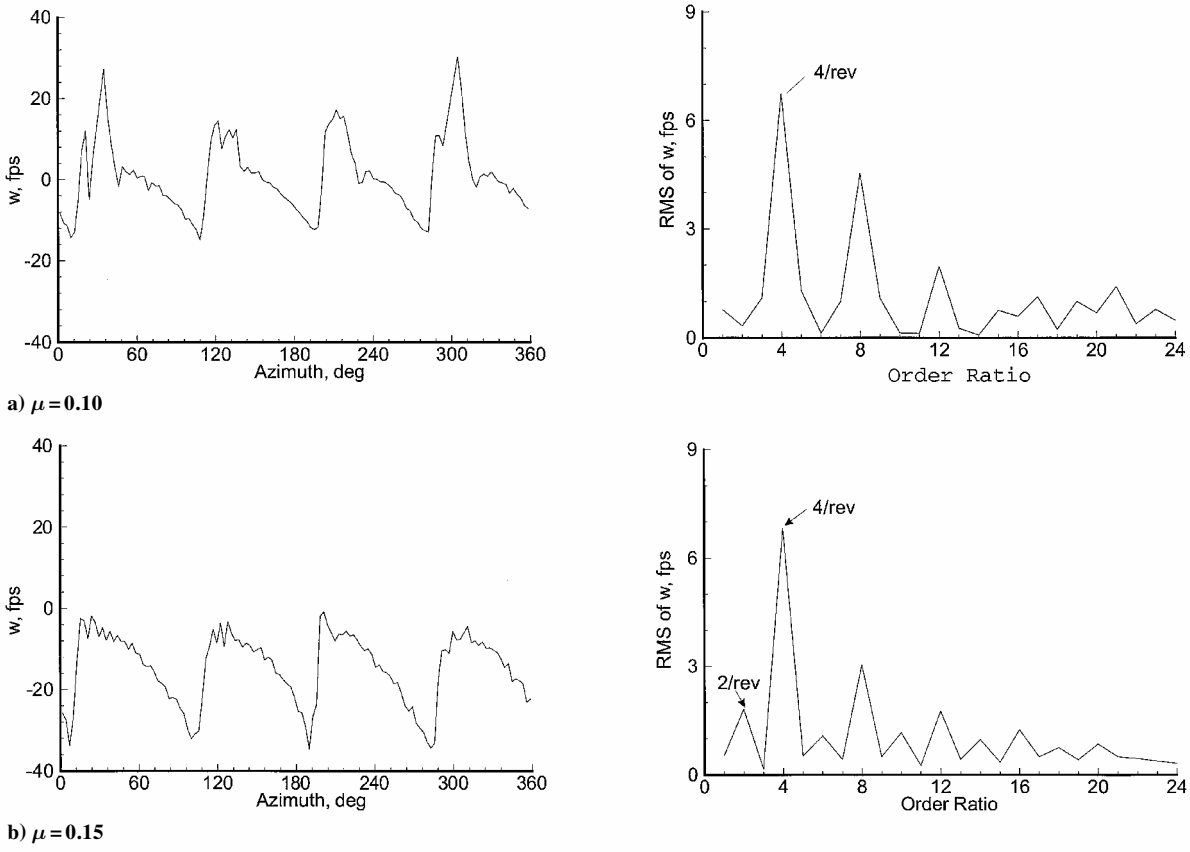

Fig. 12 Velocity and order ratio analysis for location 2 in. below centerline of horizontal tail.

the inflow studies of Refs. 46–48, 2 per revolution frequencies were noted in several instances; it is possible these frequencies are generated by vorticity shed from the hub and pylon that moves into the measurement area at the increased advance ratios.

Conclusions

To investigate the rotor wake–fuselage–empennage interactions near the empennage of a powered small-scale helicopter with an operating tail fan and a T tail, the U.S. Army Joint Research Program Office, Aeroflightdynamics Directorate, in cooperation with NASA Langley Research Center, conducted a wind-tunnel test program in the 14- by 22-Foot Subsonic Tunnel. Velocity data were acquired forward of the horizontal tail for four flight conditions, documenting the unsteady downwash and sidewash near the horizontal tail. The major conclusions from this study are as follows.

1) The horizontal tail surface experiences extremely large changes (over 30 deg) in the unsteady sidewash and downwash angles at the rotor fundamental blade passage frequency due to the influence of the rotor wake tip vortex passage. The unsteady angle variation is not captured by steady analysis of the configuration.

2) Although rotor–empennage interactions are usually encountered at very low advance ratios, for a T-tail configuration, the interaction occurs at higher advance ratios. For this configuration, the horizontal tail is most affected by the rotor wake above advance ratios of 0.10.

3) The skew angle can be calculated more accurately from the momentum equation when the forward flight velocity dependence is considered.

References

[1]Sheridan, P. F., and Smith, R. P., "Interactional Aerodynamics—A New Challenge to Helicopter Technology," American Helicopter Society, AHS Paper 79-59, May 1979.

[2]Roesch, P., and Vuillet, A., "New Designs for Improved Aerodynamic Stability on Recent Aerospatiale Helicopters," *Proceedings of the 37th Annual Forum*, American Helicopter Society, New Orleans, LA, 1981, pp. 263–275.

[3]Prouty, R. W., and Amer, K. B., "The YAH-64 Empennage and Tail Rotor—A Technical History," *Proceedings of the 38th Annual Forum*, American Helicopter Society, Anaheim, CA, 1982, pp. 247–261.

[4]Ahmed, S. R., Raddatz, J., and Hoffman, W., "Analysis of Helicopter Rotor-Fuselage Interference with Time Averaged Pressure Distribution," *Proceedings of the 17th European Rotorcraft Forum*, Berlin, Germany, 1991.

[5]Ahmed, S. R., and Meyer, F. W., "A Mach-Scaled Powered Model For Rotor-Fuselage Interactional Aerodynamics and Flight Mechanics Investigations," *Proceedings of the International Specialists' Meeting on Rotorcraft Basic Research*, American Helicopter Society, Atlanta, GA, 1991, pp. 36.1, 36.2.

[6]Bettschart, N., Hanotel, R., Ilbas, D., and Desopper, A., "Theoretical and Experimental Studies of Helicopter Rotor/Fuselage Interaction," Office National d'Etudes et de Recherches Aerospatiales, TP 1991-198, Saint-Louis, France, Jan. 1991.

[7]Norman, T. R., and Yamauchi, G. K., "Full-Scale Investigation of Aerodynamic Interactions Between a Rotor and Fuselage," *Proceedings of the 47th Annual Forum*, American Helicopter Society, Phoenix, AZ, 1991, pp. 461–486.

[8]Berry, J. D., "RWF Rotor–Wake–Fuselage Code Software Reference Guide," NASA TM-104078, July 1991.

[9]Leishman, J. G., and Bi, N. P., "Measurements of a Rotor Flowfield and the Effects on a Fuselage in Forward Flight," *Proceedings of the 16th European Rotorcraft Forum*, Glasgow, Scotland, 1990.

[10]Lorber, P. F., and Egolf, T. A., "An Unsteady Helicopter Rotor–Fuselage Aerodynamic Interaction Analysis," *Journal of the American Helicopter Society*, Vol. 35, No. 3, 1990, pp. 32–42.

[11]Meyer, F. W., "The Influence of Interactional Aerodynamics of Rotor–Fuselage–Interference on the Fuselage Flow," *Vertica*, Vol. 14, No. 2, 1990, pp. 201–215.

[12]Dehondt, A., and Toulmay, F., "Influence of Fuselage on Rotor Inflow Performance and Trim," *Vertica*, Vol. 14, No. 4, 1990, pp. 573–585.

[13]Wilson, F. T., "Fuselage Aerodynamic Design Issues and Rotor/Fuselage Interactional Aerodynamics. Part 1: Practical Design Issues," AGARD, Aerodynamics of Rotorcraft, Rept. N91-18048, Nov. 1991.

[14]Rand, O., and Gessow, A., "Model for Investigation of Helicopter Fuselage Influence on Rotor Flowfields," *Journal of Aircraft*, Vol. 26, May 1989, pp. 401, 402.

[15]Trept, T., "A 0.15-Scale Study of Configuration Effects on the Aerodynamic Interaction Between Main Rotor and Fuselage," NASA CR-166577, Jan. 1984.

[16]van Dam, C. P., Budge, A. M., and Duque, E. P. N., "A Comparison of Computed and Experimental Flowfields of the RAH-66 Helicopter," NASA CR-200906, Jan. 1996.

[17]Rajagopalan, R. G., "Procedure for Rotor Performance, Flowfield, and Interference: A Perspective," AIAA Paper 2000-0116, Jan. 2000.

[18]Egolf, T. A., Wake, B. E., and Berezin, C., "Recent Rotor Wake Simulation and Modeling Studies at United Technologies Corporation (Invited)," AIAA Paper 2000-0115, Jan. 2000.

[19]Hariharan, N., and Sankar, L. N., "A Review of Computational Techniques for Rotor Wake Modeling," AIAA Paper 2000-0114, Jan. 2000.

[20]Gmelin, B., and Philippe, J. J., "DLR/ONERA Common Program on Rotorcraft Research," AIAA Paper 2001-5201, Oct. 2001.

[21]Boyd, D. D., Jr., Barnwell, R. W., and Gorton, S. A., "Computational Model for Rotor–Fuselage Interactional Aerodynamics," AIAA Paper 2000-0254, Jan. 2000.

[22]Huber, H., and Polz, G., "Studies on Blade-to-Blade and Rotor-Fuselage-Tail Interferences," *Aircraft Engineering*, Vol. 55, Oct. 1983, pp. 2–12.

[23]Fitzgerald, J., and Kohlhepp, F., "Research Investigation of Helicopter Main Rotor/Tail Rotor Interaction Noise," NASA CR-4143, May 1988.

[24]Jacobs, E. W., Fitzgerald, J. M., and Shenoy, R. K., "Acoustic Characteristics of Tail Rotors and the Effects of Empennage Interactions," *Proceedings of the 43rd Annual Forum*, American Helicopter Society, Saint Louis, MO, 1987, pp. 437–451.

[25]Balch, D. T., "Experimental Study of Main Rotor Tip Geometry and Tail Rotor Interactions in Hover," NASA CR-177336, Feb. 1985.

[26]Balch, D. T., Saccullo, A., and Sheehy, T. W., "Experimental Study of Main Rotor/Tail Rotor/Airframe Interactions in Hover," NASA CR-166485, June 1983.

[27]Edwards, B. D., Peryea, M. A., and Brieger, J. T., "0.15 Scale Model Studies of Main and Tail Rotor Interaction," *Proceedings of the National Specialists' Meeting on Aerodynamics and Aeroacoustics*, American Helicopter Society, Arlington, TX, 1987.

[28]Martin, R. M., Burley, C. L., and Elliott, J. W., "Acoustic Test of a Model Rotor and Tail Rotor: Results for the Isolated Rotor and Combined Configuration," NASA TM-101550, Feb. 1989.

[29]Pagnano, G., and Saporiti, A., "Current European Research Activities in Helicopter Interactional Aerodynamics," *Proceedings of the 17th European Rotorcraft Forum*, Berlin, Germany, Sept. 1991.

[30]Philippe, J., "ONERA Makes Progress in Rotor Aerodynamics, Aeroelasticity, and Acoustics," *Vertiflite*, Vol. 38, No. 5, 1992, pp. 48–53.

[31]Torok, M. S., and Ream, D. T., "Investigation of Empennage Airloads Induced by a Helicopter Main Rotor Wake," *Proceedings of the 49th Annual Forum*, American Helicopter Society, Saint Louis, MO, 1993.

[32]Moedersheim, E., and Leishman, J. G., "Investigation of Aerodynamic Interactions Between a Rotor and a T-Tail Empennage," International Aeromechanics Specialists' Conf., 2nd—Aeromechanics Technology and Product Design for the 21st Century, American Helicopter Society, Bridgeport, CT, Oct. 1995.

[33]Keys, C., Sheffler, M., Weiner, S., and Heminway, R., "LH Wind Tunnel Testing: Key to Advanced Aerodynamic Design," *Proceedings of the 47th Annual Forum*, American Helicopter Society, Phoenix, AZ, 1991, pp. 77–87.

[34]Gentry, G. L., Quinto, P. F., Gatlin, G. M., and Applin, Z. T., "The Langley 14- by 22-Foot Subsonic Tunnel: Description, Flow Characteristics, and Guide for Users," NASA TP-3008, Sept. 1990.

[35]Phelps, A. E., and Berry, J. D., "Description of the Army's 2-Meter Rotor Test System," NASA TM-87762, Feb. 1987.

[36]Duque, E. P. N., Berry, J. D., Budge, A. M., and Dimanlig, A. C. B., "A Comparison of Computed and Experimental Flowfields of the RAH-66 Helicopter," International Aeromechanics Specialists' Conf., 2nd—Aeromechanics Technology and Product Design for the 21st Century, American Helicopter Society, Bridgeport, CT, Oct. 1995.

[37]Gorton, S. A., Poling, D. R., and Dadone, L., "Investigation of Blade–Vortex Interaction Using Laser Velocimetry and Pressure-Instrumented Rotor Blades. Volume 1—Advance Ratio of 0.2, Rotor Lift Coefficient Normalized by Solidity of 0.07, and Shaft Angle of 0 Degrees," NASA TM-4570, Jan. 1995.

[38]Mace, W. D., Jr., Elliott, J. W., Blancha, B., and Murphy, J., "Comparison of Frequency Domain and Time Domain Laser Velocimeter Signal Processors," *14th International Congress on Instrumentation in Aerospace Simulation Facilities*, Rockville, MD, 1991, pp. 103–112.

[39]Heyson, H. H., "Use of Superposition in Digital Computers to Obtain Wind-Tunnel Interference Factors for Arbitrary Configurations, with Particular Reference to V/STOL Models," NASA TR-R-302, Feb. 1969.

[40]"Instruments and Apparatus. Part I—Measurement Uncertainty," American National Standards Inst./American Society of Mechanical Engineers, ANSI/ASME Performance Test Codes 19.1-1985, United Engineering Center, New York, NY, 1985, pp. 3–33.

[41]Young, W. H., Jr., Meyers, J. F., and Hepner, T. E., "Laser Velocimeter Systems Analysis Applied to a Flow Survey Above a Stalled Wing," NASA TN-D-8408, Aug. 1977.

[42]Dring, R. P., "Sizing Criteria for Laser Anemometry Particles," *Journal of Fluids Engineering*, Vol. 104, March 1982, pp. 15–17.

[43]Gorton, S. A., Berry, J. D., Hodges, W. T., and Reis, D. G., "Flow Environment Study Near the Empennage of a 15-Percent Scale Helicopter Model," NASA TP-2000-210085, March 2000.

[44]Stepniewski, W. Z., and Keys, C. N., *Rotary-Wing Aerodynamics*, 1st ed., Dover, New York, 1984, pp. 62–65.

[45]Ghee, T. A., Berry, J. D., Zori, L. A. J., and Elliott, J. W., "Wake Geometry Measurements and Analytical Calculations on a Small-Scale Rotor Model," NASA TP-3584, Aug. 1996.

[46]Elliott, J. W., Althoff, S. L., and Sailey, R. H., "Inflow Measurements Made with a Laser Velocimeter on a Helicopter Model in Forward Flight—Volume I: Rectangular Planform at an Advance Ratio of 0.15." NASA TM-100541, April 1988.

[47]Elliott, J. W., Althoff, S. L., and Sailey, R. H., "Inflow Measurements Made with a Laser Velocimeter on a Helicopter Model in Forward Flight—Volume II: Rectangular Planform at an Advance Ratio of 0.23," NASA TM-100542, April 1988.

[48]Elliott, J. W., Althoff, S. L., and Sailey, R. H., "Inflow Measurements Made with a Laser Velocimeter on a Helicopter Model in Forward Flight—Volume III: Rectangular Planform at an Advance Ratio of 0.30," NASA TM-100543, April 1988.